# Optimal Design of Electrical Drive and Power Converter for Hybrid Electric Powertrain

Zhenwei WU[1,3], Daniel DEPERNET[2,3], Christophe ESPANET[1,3], Member, IEEE
[1]University of Franche-Comte, FEMTO-ST, Belfort, France
[2]University of Technology of Belfort-Montbeliard, FEMTO-ST, Belfort, France
[3]MEGEVH French National Network on Hybrid Electrical Vehicles

***Abstract*— A modeling and design method of electrical drive and power converter applied to a powertrain for a heavy duty Series-Parallel Hybrid Electric Vehicle (HEV) is described in this paper. A Surface-Mounted Permanent Magnet Synchronous Motor (SMPMSM) is considered and the motor performances are validated with Finite Element Method (FEM) simulations. Moreover, the authors investigated an optimization strategy focused on multi-criteria optimization, taking into account electrical motor modeling, electromechanical behavior modeling and the overall losses modeling including motor losses and converter losses. The optimization of the powertrain is achieved realizing a compromise between the efficiency and the motor weight minimization.**

***Keywords- Hybrid Electric Vehicle; Analytical Model; Surface-Mounted Permanent Magnet Synchronous Motor (SMPMSM); Inverter; Finite Element Method (FEM); Optimization***

## I. INTRODUCTION

The objective of the work described in this paper is to develop a hybrid powertrain [1-2] applied to a heavy duty vehicle for both military and civil applications. Figure. 1 illustrates the two applications and in these cases, the vehicle should have the following several particular performances:

- the vehicle start up should be very fast;
- As a consequence, the acceleration time should be very low;
- the vehicle could be started even for very low temperature (-35°C);
- the vehicle has to be able to work in full electric mode.

According to these reasons, a series-parallel HEV [3] architecture (see Figure 1. ) has been chosen among the 4 classical types. More precisely, the paper focuses on the power converter and the electrical motorization of the hybrid powertrain. Various electrical machine topologies applied to HEVs are described in [4]. The surface-mounted permanent magnet synchronous motor (SMPMSM) [5] has been chosen due to its simplicity of construction even if the authors are aware that the flux weakening range is relatively small and that it can lead to over-sized inverter. However, the flux weakening has been carefully evaluated, to optimize the efficiency of the whole system (converter and motor). To achieve the torque control and flux weakening, the current is controlled by using a Pulse Width Modulation (PWM) 2 levels Voltage Source Inverter (VSI) [6-7].

## II. ANALYTICAL MODELING

Many authors have developed analytical modeling of SMPMSM [8-11] since several years. In this study the analytical model was developed with MATHCAD software. To have a good representation of the motor real operating, only three working points have been considered. Those working points are presented in the Figure 2 of electrical motor characteristic and they are defined by the vehicle specifications:

- Point 1: The rotational speed is 334 rpm and the maximal transient torque is 2000 N.m. This working point corresponds to the boost operating mode. The vehicle can accelerate from 0 to 30 km/h in less than 30s. Then an additional torque of 400 N.m will be also supplied by the internal combustion engine (ICE).

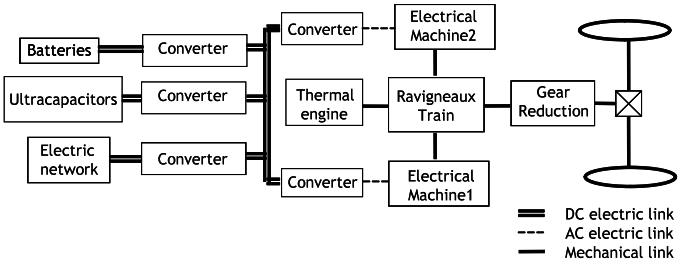


Figure 1. Structure of Series-Parallel HEV

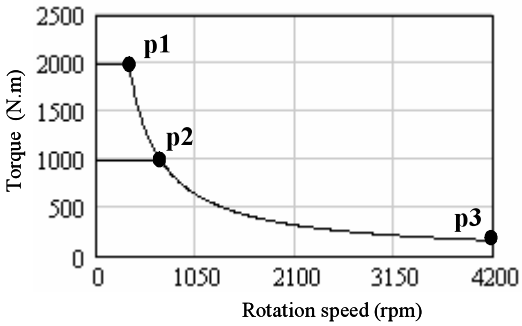


Figure 2. Working points applied

978-1-4244-8218-4/10/$26.00 ©2010 IEEE

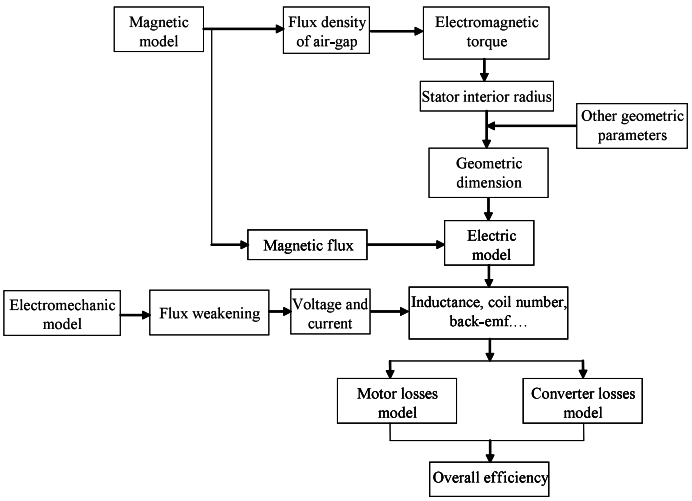


Figure 3. Global architecture of analytical modeling

- Point 2: The rotation speed is 668 rpm and the permanent torque is 1000 N.m. This working point corresponds to the rated working.
- Point 3: The maximal rotation speed is 4200 rpm and the corresponding minimum torque is 159 N.m. This working point corresponds to the over speed working.

According to the real HEV specifications, a power ratio of 1/10 has been considered to design a first prototype and to achieve an experimental studying in order to validate the design tools and the models. Then the analytical model was based on a mechanical power of 7 kW. Thus in this study, the maximal transient torque equals to 200 N.m for boost operation, 100 N.m for permanent torque on rated operation and 15.9 N.m for over speed operation. Figure 3 presents the global architecture of analytical modeling including the geometry modeling, magnetic modeling, electric modeling, electromechanical modeling, cooling system modeling and overall losses modeling.

### *A. Geometry modeling of motor*

Using an inverse modeling, the geometric sizes are deduced from the specifications.

The electromagnetic torque can be expressed as follows:

$$C_{em} = \pi \cdot r_s^{\,2} \cdot l_r \cdot B_g \cdot d_s \cdot J_s \cdot K_r \cdot K_b \,, \qquad (1)$$

where $d_s$ is the slot depth, $l_r$ is active length of motor, $J_s$ is the RMS current density in one slot, $K_r$ is the slot filling ratio (in this study an arbitrary choice of $K_r$ =1/3 has been made), $K_b$ is the winding factor. The parameter $B_g$ represents the flux density in the air-gap, which is expressed in the magnetic modeling present further in the paper. Thus the stator interior radius $r_s$ can be deduced from the torque using equation (2):

$$r_s = \left(\frac{C_{em} \cdot R_{rl}}{J_s \cdot K_r \cdot B_g \cdot R_{dr} \cdot \pi}\right)^{\frac{1}{4}} \qquad (2)$$

In this expression, $R_{dr}$ represents the ratio of slot depth to stator interior radius, $R_{rl}$ the ratio of stator interior radius to active length of motor. The geometric structure is shown in Figure 4. The magnet shape has been optimized in order to cancel harmonics of back-EMF (leading to a sinusoidal waveform) and to keep the same first harmonic amplitude than the one obtain with the initial magnet shape. This choice leads to a reduction of the cogging torque too. The final shape is not presented in this digest due to confidentiality reasons.

### *B. Magnetic Modeling*

The magnetic model is focused on analysis of the magnetic field in the various parts of the machine. The permanent magnet [12] creates the no-load magnetic field and the no-load air-gap flux density can be expressed by applying the Ampere law:

$$B_g = B_r \frac{e_{mg} / \mu_r}{K_c g + e_{mg} / \mu_r} \qquad (3)$$

where $\mu_r$ is the relative magnetic permeability, $B_r$ =1.2 T is the remanent flux density. The parameter $e_{mg}$ represents the ratio of magnet thickness to effective air-gap. The effective air-gap can be classically obtained by means of the Carter coefficient.

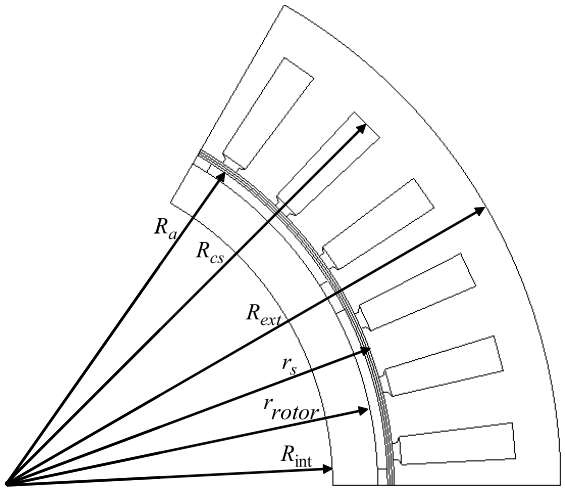


Figure 4. Geometric structure of SMPMSM

(a)

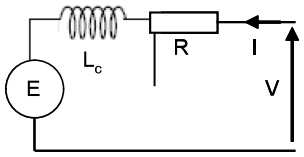


(b)

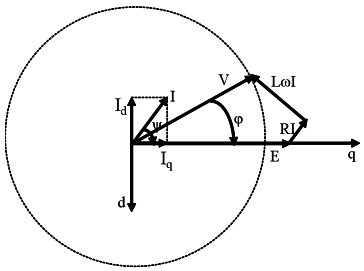


Figure 5. (a) Electric circuit of mono-phase and (b) Fresnel Diagram

Then the magnetic flux of one phase, considering only one turn per coil, can be expressed as follows:

$$\Phi_{s1} = 2K_b N_{epp} B_g r_s l_r \tag{4}$$

where $N_{epp}$ is the slot number per pole per phase. Then the total magnetic flux of one phase can be deduced:

$$\Phi_s = N_{ce}\Phi_{s1} \tag{5}$$

where $N_{ce}$ represents the number of turns in one coil.

## C. Electric Modeling

In the electric circuit presented in Figure 5 (a), the phase difference φ between the supply voltage V and the current I can be determined by means of the following relation:

$$\varphi = \arccos\left(\frac{\Phi_{s1}\cdot\omega\cdot N_{ce} + R_{s1}\cdot AT\cdot N_{ce}}{V}\right) \tag{6}$$

where ω represents the electric pulsation and $AT$ the ampere turns that can be defined by this relation:

$$AT = J_s S_{enc} K_r \tag{7}$$

According to the Fresnel diagram presented in Figure 5 (b), we can also determine as the number of turns $N_{ce}$:

$$N_{ce} = \frac{V}{\sqrt{(\Phi_{s1}\cdot\omega + R_{s1}\cdot AT)^2 + (L_{c1}\omega\cdot AT)^2}} \tag{8}$$

The parameters $R_{s1}$ and $L_{c1}$ represent the resistance and the cyclic inductance respectively, considering only one turn per coil.

Lastly, the no-load back EMF can be expressed using the following relation:

$$E_{eff} = \omega_{\dim}\Phi_s \tag{9}$$

## D. Electromechanical Modeling

While the rotation speed is less than rated rotational speed, the phase difference ψ between the current I and the back-EMF E always equals to 0, leading to the minimal copper losses for a given torque to provide. The equation (10) describes Figure 5 and electromechanical modeling, with $I = I_d + jI_q$ and where p is the poles pair number, Ω the angular speed, $C_{em}$ the electromagnetic torque, $\Phi_{eff}$ the magnetic flux RMS value and $I_{eff}$ the current RMS value of one phase.

$$\begin{cases} \underline{V} = \underline{E} + (R + jL_c\cdot p\cdot\Omega)\cdot\underline{I} = V_d + jV_q \\ C_{em} = 3\cdot p\cdot\Phi_{eff}\cdot I_{eff}\cdot\cos(\psi) \end{cases} \tag{10}$$

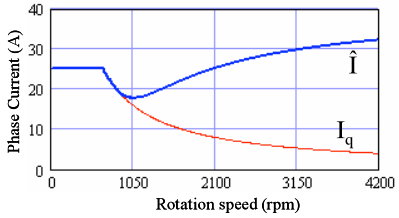


Figure 6. Influence of the phase current

Due to the electromagnetic torque profile (see Figure 2. ) and the feeding voltage limitation, flux weakening is necessary increase the speed range at constant power. The flux weakening is achieved by applying negative $I_d$ component in order to reduce the total flux of in one phase. The supply voltage is limited by the DC-link input voltage $V_{bus.}$:

$$V_{\max} = \frac{V_{bus}}{2} \tag{11}$$

In Figure 5, the Fresnel diagram shows the limitation of the supply voltage. For low rotational speeds, the phase difference between the back-EMF and the current equals to 0 and Id current is null because none flux weakening is required. The $I_q$ current is also nearly constant during this operation phase to provide the constant torque. When the rotational speed becomes higher that the one of working point 2, the torque is reduced and flux weakening may be required if the the motor voltage V reaches the maximum voltage $V_{max}$. In this case, the Id current is not null and the magnetic flux created by Id current reduces the magnetic flux created by permanent magnets. Then, the back-EMF is not in phase with the current. The evolution of the current RMS value in one phase is shown in Figure 6:

- The current $I_q$ is constant while the torque is constant. In this case, flux weakening is not required and $I_d$ equals to 0.

  For high speeds, the torque decreases, thus the current $I_q$ decreases too. The magnetic flux created by stator winding current $I_d$ increases in order to reduce the active flux created by the permanent magnets and to maintain the voltage V under the maximum value $V_{max}$. The machine flux weakening capability depends on the cyclic inductance value. Indeed, the $I_d$ current can increase a lot if the cyclic inductance is small. Then the cyclic inductance is a key point to limit the $I_d$ current at high speed and the corresponding copper losses.

*E. Overall losses modeling*

Due to the assumption that the mechanical losses and the rotor yoke losses are neglected, the global losses consist in:

- the iron and copper losses of the electrical motor;
- the inverter losses, due to the conduction and commutation losses in the IGBT transistors and the diodes.

*1) Electrical Motor Losses Modeling*

The evaluation of the electrical motor losses [13] includes:

- The calculation of iron losses in the stator teeth.
- The calculation of iron losses in the stator yoke.
- The copper losses in the windings.

For accurate calculations, the effect of flux weakening is considered in order to calculate the iron losses in the electrical motor taking into account the reduction of stator flux density due to flux weakening.

Thus the flux density in the different parts of the motor should depend on the $I_d$ current and then the electrical motor iron losses depend on both rotational speed and $I_d$ current.

The calculations have been done by the following equations with some parameters presented in the Table I:

The eddy currents coefficient is created such as:

$$k_f = \frac{{e_{stat}}^2 \cdot \sigma_{stat}}{24 \cdot mv_{stat}} \tag{12}$$

According to limit the iron losses, the authors choose the material M270-35A like stator sheet, here $e_{stat}$ is each sheet thickness of stator, $\sigma_{stat}$ is conductivity of stator sheet and $mv_{stat}$ is mass density.

The hysteresis coefficient is expressed:

$$k_h = \frac{P_{fe0} - k_f \cdot {\omega_0}^2 \cdot {B_{\max 0}}^2}{\omega_0 \cdot {B_{\max 0}}^2} \tag{13}$$

Here $P_{fer0}$ represents the irons losses is 2.7 watts per kilogram at point where the flux density $B_{max0}$ is 1.5 T and the frequency is 50 Hz, thus $\omega_0$ represents the pulsation corresponds to this frequency.

The average value of resulting magnetic flux $B_{statc}$ in the stator teeth and the stator yoke considering the flux wakening (rated-load operation) is expressed:

$$B_{statc} = B_{statv}\left(1 - \frac{L_c \cdot I_d}{\sqrt{2} \cdot \Phi_s}\right) \tag{14}$$

Here $B_{statv}$ is the magnetic flux density in the stator, which is created by magnet without the current influence (no load operation). $\Phi_s$ is the RMS value of magnetic flux of one phase, which is created by magnet without the current influence (no load operation). $L_c$ is cyclic inductance and $I_d$ is the current created by stator winding on direct axe. Then the expression $L_c$ $I_d$ describes the magnetic flux created by the stator winding current while the motor operates on rated-load.

Thus the hysteresis component of iron losses is expressed by:

$$P_{hys} = k_h \cdot \omega \cdot {B_{statc}}^2 \cdot mv_{stat} \cdot V_{stat} \tag{15}$$

And the eddy currents component of iron losses is expressed by:

$$P_f = k_f \cdot \omega^2 \cdot {B_{statc}}^2 \cdot mv_{stat} \cdot V_{stat} \tag{16}$$

Then the total stator iron losses are expressed by:

$$P_{fer} = P_{hys} + P_f \tag{17}$$

The copper losses in the motor windings are expressed by:

$$P_J = n_{ph} \cdot R_s \cdot {I_{eff}}^2 \tag{18}$$

These parameters are used to evaluate the global efficiency of electrical motor and inverter together. The multi-criteria optimization strategy is used to design the motor by respecting the target of global efficiency defined in the specifications.

*2) Inverter Losses Modeling*

The inverter losses include the diode losses and the transistor losses. The inverter losses are expressed as a function of the electrical parameters assuming a sinusoidal current. As mentioned above, the evolution of inverter current as a function of the control law is calculated with the electromechanical model. The technical parameters of IGBT and diodes used in the inverter, the DC-link voltage and the

current in the electrical motor are the input parameters of the inverter losses model.

The Table II gives the characteristics in the case of Semikron IGBT modules of reference SKM600GB066D.

The conduction losses in each IGBT are expressed by means of the instantaneous power integration during one electrical period T, such as:

$$P_{condT} = \frac{1}{T} \cdot \int_0^T V_{CEsat} \cdot I_T(t) \cdot dt \quad (1)$$

TABLE I. PARAMETERS OF IRON LOSSES

| Parameter | Symbol | Value |
|---|---|---|
| Thickness of stator iron sheet | $e_{stat}$ | 0.35 mm |
| Conductivity of stator iron sheet | $\sigma_{stat}$ | 2325581 $\Omega^{-1}m^{-1}$ |
| Iron mass density of stator | $mv_{stat}$ | 7650 $kg/m^3$ |
| Specific iron losses at 1.5 T and at 50 Hz | $P_{fe0}$ | 2.7 $W/kg$ |
| Pulsation at 50 Hz for iron losses at 1.5 T | $\omega_0$ | 314 Hz |
| Maximum flux density at 50 Hz | $B_{max0}$ | 1.5 T |

TABLE II. CHARACTERISTICS OF TRANSISTOR IGBT

| Parameter | Symbol | Value |
|---|---|---|
| Voltage constructor of measurement of $E_{on}$, $E_{off}$ | $V_{Eon\_off}$ | 300V |
| Current constructor of measurement of $E_{on}$, $E_{off}$ | $I_{Eon\_off}$ | 600A |
| Energy dissipated by starting the IGBTs | $E_{on}$ | $7.5 \cdot 10^{-3} J$ |
| Energy dissipated by extinction the IGBT | $E_{off}$ | $29.5 \cdot 10^{-3} J$ |
| Direct voltage Chute of the IGBTs | $V_{CEsat}$ | 1.9V |
| Commutation frequency | $F_{com}$ | 10000Hz |
| Direct voltage Chute of the Diodes | $V_{F0}$ | 1V |
| Energy dissipated by extinction the Diodes | $E_{rr}$ | $25 \cdot 10^{-3} J$ |
| DC-link input voltage | $V_{bus}$ | 540V |

Assuming a sinusoidal modulation, the PWM duty cycle is expressed as:

$$\alpha(t) = \frac{1}{2} + m \cdot \sin(\omega t + \varphi) \quad (2)$$

where m represents the modulation rate and φ the phase angle between the voltage and the current of the same phase. We can then deduce the current in the IGBT as a function of the phase current and then the conduction losses in each IGBT. They were given through the expression undermentioned where Imax and Vmax are respectively the phase current amplitude and the phase voltage amplitude, such as:

$$P_{condT} = \frac{V_{CEsat} \cdot I_{max}}{2} \cdot \left[ \frac{1}{\pi} + \frac{V_{max}}{2 \cdot V_{bus}} \cdot \cos(\varphi) \right] \quad (3)$$

The IGBT commutation losses are obtained by extrapolating the value of dissipation energy given by the constructor and assuming their linear dependency with the voltage and the current observed during the commutations. Thus the switch on dissipation power in the IGBT is defined as the overall dissipation energies at the switch on during one second, expressed such as:

$$P_{onT} = \sum_{i=1}^{N(1s)} E_{on} \frac{I(i)}{I_{Eon\_off}} \cdot \frac{V_{bus}}{V_{Eon\_off}} \quad (4)$$

Assuming the distribution of commutations as uniform, the switch on losses in the IGBT is expressed by the following equation:

$$P_{onT} = \frac{E_{on} \cdot I_{max} \cdot V_{bus}}{\pi \cdot I_{Eon\_off} \cdot V_{Eon\_off}} \cdot F_{com} \quad (5)$$

By using the same method for the extinction IGBT losses calculation, the following equation is obtained:

$$P_{offT} = \frac{E_{off} \cdot I_{max} \cdot V_{bus}}{\pi \cdot I_{Eon\_off} \cdot V_{Eon\_off}} \cdot F_{com} \quad (6)$$

Thus the total losses of IGBT can be expressed by the equation:

$$P_T = P_{condT} + P_{onT} + P_{offT} \quad (7)$$

The losses in the diodes can be obtained through the same method of calculation above, and by considering a complementary conduction to the conductions of IGBT in each interval of carrier period. Thus the equations

undermentioned permit to express the losses by conduction and by commutation in each diode of inverter:

$$P_{condD} = \frac{V_{FO} \cdot I_{\max}}{2} \cdot \left[ \frac{1}{\pi} - \frac{V_{1\max}}{2 \cdot V_{bus}} \cdot \cos(\varphi) \right] \quad (8)$$

$$P_{comD} = \frac{E_{rr} \cdot I_{\max} \cdot V_{bus}}{\pi \cdot I_{Eon\_off} \cdot V_{Eon\_off}} \cdot F_{com} \quad (9)$$

The total losses of diodes can be expressed as:

$$P_D = P_{condD} + P_{comD} \quad (10)$$

Finally, we deduced the total losses in the semi-conductors of inverter, such as:

$$P_{ond} = 6 \cdot (P_D + P_T) \quad (11)$$

### *F. Cooling system analysis*

The electrical motor and the converter will be cooled by using the same water circuit. The cooling system is characterized by the following parameters: input temperature of electrical motor $T_{in}$; pressure of water circuit $P_r$; fluid flow D and maximal temperature gradient $\Delta T$ between input and output of each component including the electrical motor and the inverter. The maximal extracted power P can be expressed as a function of the temperature gradient $\Delta T$:

$$P = d \cdot D \cdot C \cdot \Delta T \quad (12)$$

where d represents the water density (d = 1 kg/l) and C represents the specific heat capacitor of water ($C \approx 4186$ $J.kg^{-1}K^{-1}$). From those previous numerical values, it is possible to deduce the maximal possible value of both motor and inverter losses that the cooling system is able to evacuate.

## III. Overall Optimization Procedure

The optimization is based on the used of a Sequential Quadratic Programming (SQP) algorithm through the software Pro@Design [14]. The global strategy is based on a multi-criteria and multi-constraints optimization, to take into account the links between the various components. All the previous models make it possible to analytically obtain the global behavior of the electrical drive train. Figure 7 shows the strategy of global modeling and optimization. The choice of optimal criterions and constraints depends on the mechanical constraints, magnetic constraints, electrical constraints, etc. To take into account the electrical motor and inverter efficiencies during the vehicle mission profiles, the efficiencies are expressed for the main working points presented in Figure 2 and they are weighted by statistic factors. The optimization is performed to make a compromise between the global efficiency and the mass of the motor, respecting all the constraints.

The used objective function J is expressed in the equation (28), it combined the different criteria that the authors have chosen to optimize, such as the different currents $I_1$, $I_2$ and $I_3$ at three working points and the motor mass $M_{mot}$.

$$J = \tau_m \cdot M_{mot} + \tau_1 \cdot I_1 + \tau_2 \cdot I_2 + \tau_3 \cdot I_3 \quad (13)$$

The weighting coefficients $\tau_m$ , $\tau_1$ , $\tau_2$ , $\tau_3$ make it possible to adapt the importance of each criterion and to optimize the various criteria at the same time. In order to obtain the maximal transient torque during the boost regime, the coefficient $\tau_1$ is necessarily considered. Each current criteria coefficient permits to minimize the global losses of motor and inverter at each working point, but it's impossible to minimize all of them. Then, the key solution is to find out the compromise coefficients, this choice depending on which improvement rate of criteria is more sensible than the others. Several intermediate optimization results have been shown in Table III, in which the motor mass and volume have been minimized by increasing the efficiencies, the final values of the prototype are presented in the last column.

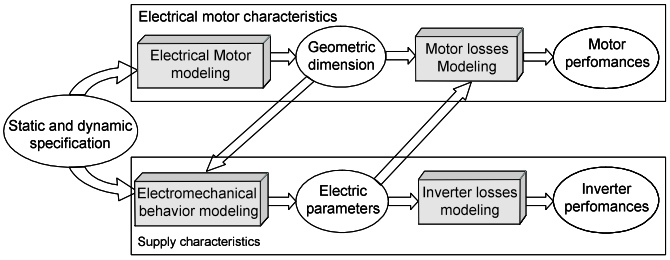


Figure 7. Optimization procedure of the global system

TABLE III. Optimization Results

| | | 1 | 2 | 3 | Proto-type |
|---|---|---|---|---|---|
| Mass | $M_{mot}$ (kg) | 74.2 | 56.7 | 47 | 44.3 |
| Volume | $V_{mot}$ (liter) | 17.7 | 13.6 | 11.3 | 10.6 |
| Current 1 | $I_1$ (A) | 26.4 | 27.3 | 28.6 | 35 |
| Current 2 | $I_2$ (A) | 13.2 | 13.6 | 14.3 | 17.5 |
| Current 3 | $I_3$ (A) | 33 | 27.8 | 24.8 | 27.3 |
| Efficiency 1 | $\eta_1$ (%) | 87 | 83.4 | 79.6 | 77.7 |
| Efficiency 2 | $\eta_2$ (%) | 93.7 | 93 | 92.1 | 91.4 |
| Efficiency 3 | $\eta_3$ (%) | 83.6 | 84.3 | 84.7 | 85.4 |

## IV. Validation by Finite Element Modelling

The validation of the motor electromagnetic performances has been performed using Finite Element Method (FEM) simulations. In particular, influence of saturation is carefully studied for boost working, since it is difficult to evaluate the local flux density and the overall magnetic flux including the magnetic flux created by permanent magnets and the stator winding currents in the analytic modeling. The magnetic saturation [9] and [15-16] can results from approximation concerning the stator and rotor magnetic characteristics, which may produce errors on the calculation of flux density, back-EMF and torque. For the analytic study and the optimizations, the flux density is limited in order to avoid the magnetic saturation. In Figure 8, we can observe that the fundamental back-EMF given by analytic model and FEM simulations are quite similar. In Figure 9, a good agreement between the torque given by analytic model (based on sinusoidal EMF) and the one given by FEM simulations is also obtained. Finally, Table IV summarizes the back-EMF first harmonic, the torque at rated speed and the maximal torque (boost working) obtained with both analytical model and FEM simulations.

TABLE IV. Comparison of Performances

| | **Analytic** | **FEM** |
|---|---|---|
| Fundamental value of back-EMF on nominal speed | 188.6 V | 190.6 V |
| Torque on nominal speed | 100 Nm | 99.8 Nm |
| Torque on boost | 200 Nm | 189.5 Nm |

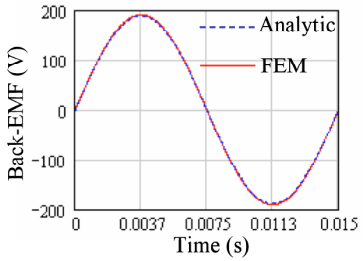


Figure 8. Comparison of fundamental value of back-EMF on nominal speed

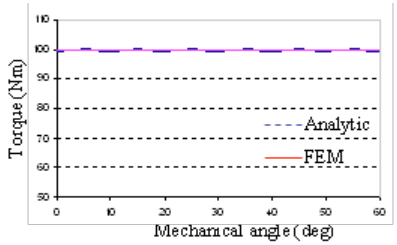


Figure 9. Comparison of torques on nominal speed

## V. Conclusion

In this paper the design of an electrical drive (inverter and PM machine) for a serial/parallel hybrid powertrain used in a heavy-duty vehicle has been proposed. The authors have described the analytical modeling including geometric, magnetic, electric and thermal models. The inverter and machine losses have been calculated in order to express the global efficiency.

Then an optimization tool has been used to achieve a compromise between the motor mass and the global efficiency. Thanks to this approach it has been possible to reduce the maximal current in the stator phases (optimization of the flux weakening), to improve the efficiency of the global system and to reduce the volume of the powertrain. After the optimization, the final motor performances of prototype based on the three working points are presented in the Table I, including the motor mass (44.3 kg) and volume (10.6 liter), the rms value of current based on 3 working points (35A, 17.5A and 27.3A) and the overall efficiency including the motor and the invertor (77.7%, 91.4% and 85.4%).

The next steps will be to include the design of the reduction gear (by using analytical models of the geometry and the losses) and to realize a global optimization of the complete powertrain. An electrical machine prototype is also under realization to validate the used model and the optimization approaches.

More details about the model and the optimization strategy will be developed in the final paper. In particular the choice of the criteria and the influence of this choice on the designed machines will be presented.

## Acknowledgment

This work has been carried out in collaboration with NEXTER SYSTEM in the framework of ARCHYBALD project of 2007 edition of PREDIT Clean and Economical Vehicles program. It has been funded by National Agency of Research (ANR) and supported by Environment and Energy Mastery Agency (ADEME).

## References

[1] Samuel P. Taylor, “Design and Simulation of High Performance Hybrid Electric Vehicle Powertrains”, Thesis of Master, College of Engineering and Mineral Resources at West Virginia University, 2001.

[2] Victor MESTER, “Conception Optimale Systémique des Composants des chaînes de Traction Electrique”, Doctoral thesis, Central School of Lille, May 2007.

[3] C.C. Chan, “The State of the Art of Electric and Hybrid Vehicles”, Proceedings of the IEEE, Vol. 90, No. 2, February 2002.

[4] Z.Q. Zhu and C.C. Chan, “Electrical Machine Topologies and Technologies for Electric, Hybrid, and Fuel Cell Vehicles”, IEEE Vehicle Power and Propulsion Conference, September 2008.

[5] Li Zhu, S.Z. Jiang, Z.Q. Zhu and C.C. Chan, “Comparison of Alternate Analytical Models for Cogging Torque in Surface-Mounted Permanent Magnet Machines”, IEEE Vehicle Power and Propulsion Conference, Septembre 2008.

[6] Stefan Laurentiu CAPITANEANU, “Optimisation de la fonction MLI d’un onduleur de tension deux-niveaux”, Thesis of doctor, Polytechnical National Institut of Toulouse, November 2002.

[7] D. Depernet, “Optimisation de la commande d’un onduleur MLI à trois niveaux de tension pour machine asynchrone” Doctoral thesis, University of Reims Champagne-Ardenne, December 1995.

[8] G. Slemon, X. Liu, “Modeling and design optimization of permanent magnet motors”, Electrical Machines and Power Systems, Vol. 20, pp.71-92, 1992.

[9] C.Espanet, “Modélisation et conception optimale de moteurs sans balais à structure inversée. Application au moteur-roue”, Doctoral thesis, University of Franche-Comte, January 1999.

[10] Gordon R.Slemon, “On the Design of High-Performance Surface-Mounted PM Motors”, IEEE Transactions on Industry Applications, Vol. 30, No. 1, pp.134-140, January/February.1994.

[11] Zhenwei Wu, Daniel Depernet, Christophe Kieffer, Frederic Dubas, Daniel Hissel, Christophe Espanet, “Electrical Motor Design for Hybrid Heavy-Duty Electrical Powertrain”, IEEE Vehicle Power and Propulsion Conference, September 2009.

[12] Luc LECHEVALLIER, Jean-Marie LE BRETON, Philippe TENAUD, Antoine MOREL, Serge BRASSARD, “Aimants permanents - Applications et perspectives”, Techniques of engineer, RefD2102, Mai 2007.

[13] Thierry GAUTREAU, “Estimation des pertes fer dans les machines électriques. Modèle d'hystérésis loss surface et application aux machines synchrones à aimants”, Doctoral thesis, Polytechnical National Institut of Grenoble, December 2005.

[14] Stéphane BRISSET, “Démarches et Outils pour la Conception Optimale des Machines Electriques”, Doctoral thesis, University of sciences and technologies of Lille", December 2007.

[15] A.M. El-Serafi, A.S. Abdallah, M.K. El-Sherbiny, E.H. Badawy, “Experimental study of the saturation and the cross-magnetizing phenomenon in saturated synchronous machines”, IEEE Transactions on Energy Conversion, Vol. 3, No. 4, pp. 815-823, December 1988.

[16] E.Levi, “Saturation Modelling in D-Q Axis Models of Salient Pole Synchronous Machines”, IEEE Transactions on Energy Conversion, Vol. 14, No. 1, pp. 44-50, March1999.